

LETTER TO THE EDITOR

The coherent motion of Cen A dwarf satellite galaxies remains a challenge for Λ CDM cosmology[★]

Oliver Müller¹, Marcel S. Pawłowski², Federico Lelli³, Katja Fahrion⁴, Marina Rejkuba⁴, Michael Hilker⁴,
Jamie Kanehisa^{2,5}, Noam Libeskind^{2,6}, and Helmut Jerjen⁷

¹ Observatoire Astronomique de Strasbourg (ObAS), Université de Strasbourg – CNRS, UMR 7550, Strasbourg, France
e-mail: oliver.muller@astro.unistra.fr

² Leibniz-Institut für Astrophysik Potsdam (AIP), An der Sternwarte 16, 14482 Potsdam, Germany

³ School of Physics and Astronomy, Cardiff University, Queens Buildings, The Parade, Cardiff CF24 3AA, UK

⁴ European Southern Observatory, Karl-Schwarzschild Strasse 2, 85748 Garching, Germany

⁵ Department of Physics, University of Surrey, Guildford GU2 7XH, UK

⁶ University of Lyon, UCB Lyon-1/CNRS/IN2P3, I2PI, France

⁷ Research School of Astronomy and Astrophysics, Australian National University, Canberra, ACT 2611, Australia

Received 23 November 2020 / Accepted 14 December 2020

ABSTRACT

The plane-of-satellites problem is one of the most severe small-scale challenges for the standard Λ cold dark matter (Λ CDM) cosmological model: Several dwarf galaxies around the Milky Way and Andromeda co-orbit in thin, planar structures. A similar case has been identified around the nearby elliptical galaxy Centaurus A (Cen A). In this Letter, we study the satellite system of Cen A, adding twelve new galaxies with line-of-sight velocities from VLT/MUSE observations. We find that 21 out of 28 dwarf galaxies with measured velocities share a coherent motion. Similarly, flattened and coherently moving structures are found only in 0.2% of Cen A analogs in the Illustris-TNG100 cosmological simulation, independently of whether we use its dark-matter-only or hydrodynamical run. These analogs are not co-orbiting, and they arise only by chance projection, thus they are short-lived structures in such simulations. Our findings indicate that the observed co-rotating planes of satellites are a persistent challenge for Λ CDM, which is largely independent from baryon physics.

Key words. dark matter – cosmology: observations – galaxies: dwarf – galaxies: elliptical and lenticular, cD – galaxies: halos – galaxies: kinematics and dynamics

1. Introduction

One of the main challenges for current models of galaxy formation is the plane-of-satellites problem (Pawłowski 2018). The plane-of-satellite problem has its roots in the mid-1970s (Kunkel & Demers 1976; Lynden-Bell 1976), even though the implications for cosmology had not been realized at that time. The then known six satellites of the Milky Way (MW) were found to be arranged in a thin, planar structure and were thought to have a tidal origin (Lynden-Bell 1982). In the beginning of the new millennium, several high-resolution cosmological simulations became available (e.g., Springel et al. 2005), which allowed for the investigation of cosmological predictions on the scale of galaxy groups. Kroupa et al. (2005) pointed out that the flattened spatial distribution of the then known eleven Milky Way satellites – a feature which was essentially discovered 40 years earlier – is incompatible with the standard Λ cold dark matter (Λ CDM) model of structure formation, which predicts nearly isotropic satellite distributions. This conclusion was met with several rebuttals (e.g., Zentner et al. 2005; Libeskind et al. 2005, 2009), showing that a certain degree

of anisotropy is imprinted in the galaxy distribution from the accretion through the cosmic web (Libeskind et al. 2016), thus some galaxies may occasionally host flattened satellite structures. The discovery of another flattened structure of satellite galaxies around the Andromeda galaxy (Koch & Grebel 2006; McConnachie & Irwin 2006) showed that these planar distributions may not be rare exceptions.

A major step in understanding these structures was the measurement of the proper motions of the classical MW satellites with the *Hubble* Space Telescope (HST, e.g., Dinescu et al. 2004; Sohn et al. 2017), revealing that these galaxies are also kinematically correlated (Metz et al. 2008; Pawłowski et al. 2012). A similar kinematic coherence was later found for the Andromeda system by measuring the line-of-sight velocities of the dwarf galaxies (Ibata et al. 2013). Novel proper motion measurements of two satellites of the Andromeda galaxy indicate that they too co-orbit along their satellite plane (Sohn et al. 2020).

Nowadays, the existence of co-rotating satellite systems represents one of the major controversies in near-field cosmology (Ibata et al. 2014a; Cautun et al. 2015; Pawłowski et al. 2015; Sawala et al. 2016; Lipnický & Chakrabarti 2017; Samuel et al. 2020). While the mere existence of flattened structures is not seen as a major problem anymore (e.g., Santos-Santos et al. 2020), the kinematic coherence of the satellite systems is a conundrum. Considering both phenomena, the spatial flattening

[★] Based on observations collected at the European Organisation for Astronomical Research in the Southern Hemisphere under ESO programmes 0101.A-0193(A) and 0101.A-0193(B).

and the kinematic coherence constitute the actual plane-of-satellites problem (Pawlowski 2018).

It is important to determine whether flattened, co-rotating satellite systems are a peculiarity of the Local Group or whether they are present around other galaxies as well. Using the Sloan Digital Sky Survey (SDSS), Ibata et al. (2014b) studied pairs of satellite galaxies on opposite sides of their host and found that their line-of-sight velocities are preferentially anticorrelated. This is expected if they lie in co-rotating planes, suggesting that planes of satellites might be abundant in the Universe if the signal is indeed physical and not a chance occurrence (Phillips et al. 2015; Cautun et al. 2015, but see also Ibata et al. 2015).

In the Local Volume ($D < 10$ Mpc), there is evidence for flattened structures around Cen A (Tully et al. 2015), M 83 (Müller et al. 2018a), and M 101 (Müller et al. 2017a). Regarding Cen A, Tully et al. (2015) suggest the existence of two almost parallel satellite planes, but the subsequent discovery of new dwarf galaxies (Crnojević et al. 2016; Müller et al. 2017b) weakened the case for a strict separation in two planes (Müller et al. 2016, 2019). Interestingly, the planes around Andromeda and Cen A are mainly aligned with the cosmic web, while the plane around the MW and the candidate planes around M 83 and M 101 are not (Libeskind et al. 2015, 2019).

In Müller et al. (2018b), we report the discovery of a kinematic correlation among the satellites of Cen A: 14 out of 16 galaxies seemingly co-rotate around the host. In cosmological simulations, satellite systems with a similar degree of kinematic coherence and flattening were found in only $\leq 0.5\%$ of Cen A analogs, indicating a similar degree of conflict as in earlier studies of the MW and Andromeda. In Müller et al. (2021), we present spectroscopy taken with the Multi Unit Spectroscopic Explorer (MUSE) mounted at the Very Large Telescope (VLT) of 12 additional dwarf galaxies around Cen A. Here we use them to test our previous assessment of a co-rotating plane-of-satellites around Cen A.

2. The Cen A satellite system

Cen A – the central galaxy of the Centaurus group – is one of the best studied nearby galaxies beyond the Local Group. To date, 27 dwarf satellites of Cen A have both accurate distances and velocity measurements. The line-of-sight velocities were measured using the following two different techniques: emission lines from atomic and/or ionized gas for star forming galaxies (e.g., Koribalski et al. 2004) or absorption line spectroscopy of the stars (e.g., Puzia & Sharina 2008; Müller et al. 2021). The distances come from tip of the red giant branch (TRGB) measurements based on HST programs (Karachentsev et al. 2007) and our VLT program (Müller et al. 2019). An additional dwarf galaxy (ESO 174–001) has a velocity measurement, but no accurate distance estimate. As we mainly focus on the motion of satellites, we include this dwarf in our sample, for a total of 28 satellites. All galaxies used in the analysis are presented in Table A.1.

There are 13 more dwarfs around Cen A which have TRGB measurements (e.g., Crnojević et al. 2019), but they lack the velocities necessary to study the kinematics of the satellite system. More than 30 additional candidates (Müller et al. 2015, 2017b; Taylor et al. 2018) await membership confirmation.

Figure 1 shows the on-sky distribution and line-of-sight velocities of the 28 satellites with respect to Cen A. If the co-rotating satellite system suggested by Müller et al. (2018b) is a real physical structure, then the dwarfs to the north of Cen A should be blueshifted, while the dwarfs to the south should be redshifted. This is the case for 21 out of 28 of the dwarf satellites.

Figure 2 presents the position-velocity diagram for the dwarf galaxies around Cen A. For convenience, we assigned positive and negative separations from Cen A to the northern and southern satellites, respectively, adopting a separating line with a position angle $PA = 95^\circ$ and the mean velocity of the group of $v = 555 \text{ km s}^{-1}$. This position angle corresponds to the geometric minor axis of the 28 satellite galaxies studied in this work. If the satellite system has significant rotational support with all the members having near-circular orbits and sharing the same orbital motion, we would expect them to populate two opposing quadrants in the position-velocity diagram. On the other hand, a pressure-supported system would fill all four quadrants equally. Figure 2 clearly favors the former case: out of 28 galaxies, 21 lie in two opposing quadrants.

If we assume that this signal arises by chance and calculate its probability via the binomial coefficient, the probability of finding exactly 21 out of 28 galaxies in opposing quadrants is $P(X = 21 | 28) = 0.88\%$, while the one of finding 21 or more out of 28 is $P(X \geq 21 | 28) = 1.26\%$. For comparison, Müller et al. (2018b) found that 14 out of 16 satellites in opposing quadrants yield a probability of $P(X = 14 | 16) = 0.36\%$ or $P(X \geq 14 | 16) = 0.42\%$. Thus, the statistical significance of a kinematic signal has nearly stayed the same after almost doubling the sample size. Therefore, it is likely that a rotational component is present in the satellite system, even though five of the new data points do not follow this pattern. Two of the latter lie in the inner region of the system, where the line-of-sight velocities are less likely to indicate the orbital direction if the satellites follow noncircular orbits.

3. Comparison to cosmological expectations

The high degree of kinematic correlation among the satellite galaxies of Cen A has been shown to be rare in cosmological simulations (Müller et al. 2018b). In the hydrodynamical Illustris simulation (Vogelsberger et al. 2014), only 0.5% of mock-observed satellite systems around hosts of a similar virial mass as Cen A were both as flattened and kinematically correlated. For the dark-matter-only Millennium-II simulation (Boylan-Kolchin et al. 2009), the frequency of analogs to the Cen A satellite system was even lower: only 0.1%. Here we update these comparisons, adding our new data to determine whether the tension with cosmological expectations remains or is alleviated given the more comprehensive observational picture.

We base our comparison on the IllustrisTNG project, specifically the TNG100-1 run (e.g., Springel et al. 2018; Pillepich et al. 2018). IllustrisTNG expands the original Illustris simulations by refining the implemented physics. The adopted cosmological parameters are consistent with a *Planck* cosmology (Planck Collaboration XIII 2016). The simulations' box size ($75 \text{ Mpc } h^{-1}$) and resolution (dark matter particle mass $m_{\text{DM}} = 7.5 \times 10^6 M_\odot$ for the hydrodynamical run) provide a good compromise between the number of hosts and the number of resolved satellites. We used the publicly available redshift zero galaxy catalogs (Nelson et al. 2019). By using both the hydrodynamical and the equivalent dark-matter-only (DMO) run, we could directly determine whether baryonic physics (as implemented in the simulation) affects the planes-of-satellites issue.

3.1. Simulated Cen A analogs and mock satellite systems

We selected Cen A analog host galaxies by a mass and isolation criterion. The simulated host halos are required to have a

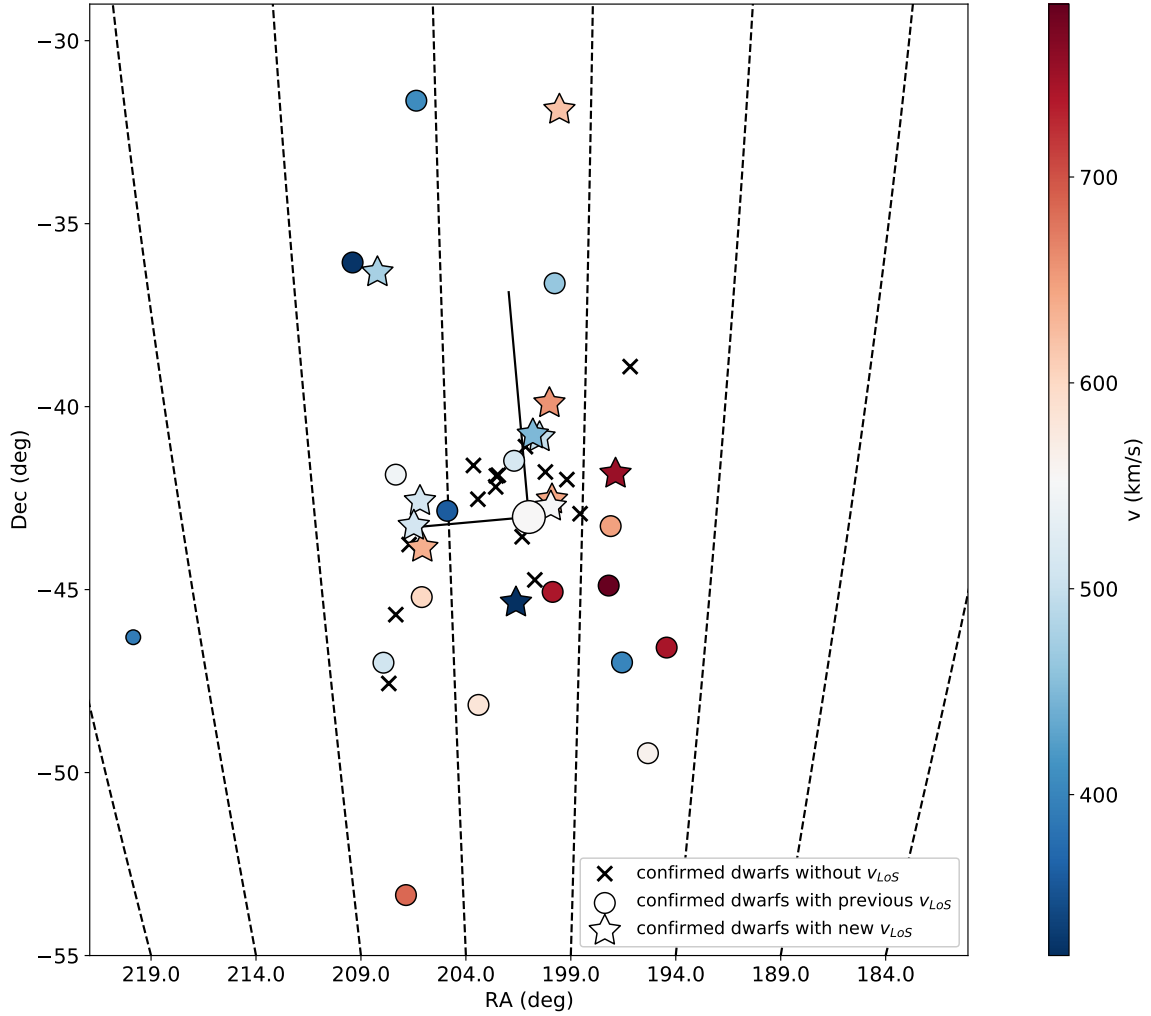


Fig. 1. On-sky distribution of the Cen A satellite system within 800 kpc. The circles correspond to the dwarf galaxies studied in Müller et al. (2018b), the stars to the newly observed dwarfs (Müller et al. 2021). The colors indicate whether the galaxies are redshifted or blueshifted with respect to the systemic velocity of Cen A (shown with a large open circle). The crosses are dwarf galaxies with known distances but without velocity information, and the small blue dot to the left is a dwarf galaxy that does not belong to the plane-of-satellites. The black lines centered on Cen A correspond to the major and minor axes of the satellite distribution.

virial mass M_{200} between 4×10^{12} and $12 \times 10^{12} M_{\odot}$. This is identical to the mass range of Cen A analogs in Müller et al. (2018b). We required each host to be isolated by rejecting any potential hosts which contain a second halo with virial mass $M_{200} \geq 0.5 \times 10^{12} M_{\odot}$ within 1.2 Mpc radius, motivated by the distance of Cen A to M 83, the second major galaxy in the Centaurus group. For each host, we identified all (subhalo) galaxies within 800 kpc as possible satellites, which is comparable to the distance range of observed satellites (see Fig. 2). It is important to note that we only selected subhalos by this volume and did not require the possible satellites to be bound to their host, since no such selection was made on the observational data either. Finally, to exclude cases of possible ongoing major mergers, we rejected all hosts which have a satellite whose stellar mass exceeds one-fourth of the host galaxy stellar mass, as these would not resemble the observed Cen A system. For the DMO run, the latter criterion was applied to the virial masses, though a smaller number of hosts was rejected in this case since dark matter mass is more easily stripped and thus reduced faster after infall. These criteria result in 180 Cen A analogs from the hydrodynamical TNG100 run and 307 from the DMO run.

In the DMO run, the satellites of a given host were ranked by their dark matter mass. In the hydrodynamical run, the satellites were ranked by their stellar mass first and then by their dark matter mass for those subhalos that do not contain stellar particles. We allowed the inclusion of such dark satellites to ensure a large sample of satellite systems with a sufficient number of satellites to compare to the observed situation, as was also done for MW analogs in Pawłowski & Kroupa (2020). It is safe to assume that the presence or absence of stars in subhalos of the dwarf-galaxy scale does not strongly affect the subhalo position or motion, given the dynamical dominance of the dark matter component. While this ensures a meaningful test of cosmological predictions, it could be improved upon in the future by comparisons with dedicated, higher-resolution zoom simulations of Cen A analogs.

We mock-observed each satellite system by placing the host at a distance of 3.68 Mpc, projecting the satellites on the sky in angular coordinates relative to the host, and calculating the line-of-sight velocity component of each satellite. Satellites were then selected in order from the ranked list requiring them to be between 1° and 12° from the host. For a comparison to the extended data set presented in this study, we required

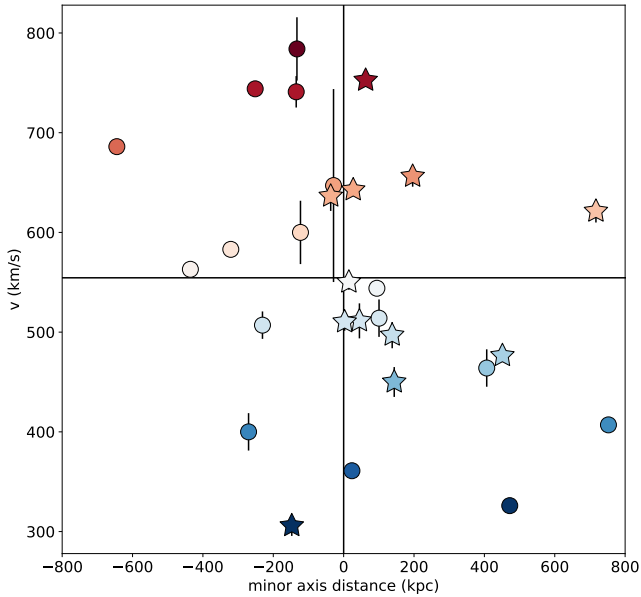


Fig. 2. Position-velocity diagram for the dwarf galaxy satellite system of Cen A. The x -axis represents the distance from the minor axis (i.e., along the major axis) derived from the satellite distribution. The filled circles show the dwarf galaxies used in Müller et al. (2018b), and the stars illustrate the new data. The uncertainties are always plotted, but often smaller than the dots. Approaching and receding galaxies with respect to the mean of the group are shown in blue and red, respectively, as in Fig. 1.

28 satellites to be selected. For each of the 180 hosts identified in the hydrodynamic TNG100 simulation, this process was repeated for ten different random viewing directions. We obtained 1763 mock-observed systems because for 37 realizations, there were less than 28 simulated satellites within the mock-observed volume around their host. For the DMO run, there were 307 hosts and 3070 mock-observed realizations.

We checked that the selected mock satellite systems had a radial root-mean-square (rms) distribution in angular coordinates on the sky, consistent with that of the observed Cen A system. For the 28 observed satellites, we found an rms radial distance from the position of Cen A of $R_{\text{rms}} = 5^{\circ}46 \pm 0^{\circ}67$ with the uncertainty determined by bootstrapping. From the hydrodynamical run, the average and standard deviation of the simulated systems with 28 satellites is $\langle R_{\text{rms}} \rangle = 5^{\circ}69 \pm 0^{\circ}64$. The DMO run tends to result in slightly more radially extended satellite systems, with an average and standard deviation of $\langle R_{\text{rms}} \rangle = 6^{\circ}33 \pm 0^{\circ}66$. This is because of a couple of reasons. The combined effect of a steeper inner density profile due to a disk, less mass loss due to tides, and a larger dynamical friction means that halos have more concentrated satellite distributions in hydrodynamical rather than DMO simulations (Libeskind et al. 2010).

3.2. Frequency of Cen A analogs in simulations

As in Müller et al. (2018b), we decided to be conservative and considered only the on-sky distribution of the simulated satellite systems and their line-of-sight velocity components. For each mock-observed system, we found the major axis of the on-sky satellite distribution and measured the rms flattening perpendicular to this direction (the minor to major axis ratio b/a). We also counted the number N_{corr} of satellite galaxies with coherent line-of-sight velocities along the major axis (i.e., consistently redshifted or blueshifted with respect to the central halo) by

dividing the on-sky satellite distribution along the minor axis. For the observed Cen A system, this yields an on-sky flattening of $b/a = 0.52$ and $N_{\text{corr}} = 21$. A slightly larger N_{corr} number might be found for a different orientation of the dividing line; however, to ensure unbiased comparisons to the simulations, we opted to define the orientation using only spatial information.

The results of our comparison for the full sample of 28 satellites is shown in Fig. 3. Considering that the frequency of both the kinematic coherence and flattening is as extreme or more than the observed Cen A satellite population (measured as f_{both}), we find that only $f_{\text{both}} = 0.3\%$ of the DMO mock systems (eight out of 3070 realizations) and $f_{\text{both}} = 0.2\%$ of the hydrodynamic mock systems (three out of 1763 realizations) are as extreme or more than the Cen A system. Thus, the inclusion of baryon physics does not alleviate the plane-of-satellites problem for Cen A. Even though the fraction of correlated satellites has dropped compared to the earlier study, the significance or rarity of this occurring in cosmological simulations remains unchanged, since we are probing a larger fraction of the total satellite population.

The fraction f_{corr} of simulated systems which are at least as kinematically correlated as observed is consistent between the DMO and hydrodynamical runs (3.2 versus 3.6%). However, the DMO run has a smaller frequency of similarly flattened satellite systems ($f_{\text{flat}} = 3.0\%$) than the hydrodynamic run ($f_{\text{flat}} = 6.6\%$). We suspect this is related to the slightly less compact radial distribution in the DMO run, as it has been found that more compact satellite systems tend to result in more flattened distributions (Pawlowski et al. 2019).

For the previous analysis, we compared our observations to the 28 brightest, or most massive in the DMO simulation, subhalos. The question remains whether the ranked selection of subhalos does bias the results. To assess this, we repeated our analysis on the TNG-100 simulation, considering the hydrodynamical run. Instead of selecting the 28 brightest subhalos, we selected the 40, 45, and 50 brightest subhalos and drew a random sample of 28 subhalos out of those. Finding 21 out of 28 coherently moving and flattened satellites as observed around Cen A occurs in 0.3%, 0.4%, and 0.1% of the simulated Cen A analogs, respectively. In other words, the frequency does not change whether we were to pick the 28 brightest subhalos or randomly draw from a larger sample of subhalos. We draw the same conclusion as in Müller et al. (2018b).

3.3. Properties of identified analogs

Figure 4 shows the three mock satellite systems in the hydrodynamical Illustris TNG simulation that are at least as flattened ($b/a \leq 0.52$) and have at least as many kinematically correlated satellites ($N_{\text{corr}} \geq 21$) as Cen A. For each of these three cases, only one out of ten random view directions results in a match. The other nine random view directions do not simultaneously reproduce the observed spatial flattening or kinematic correlation. This suggests that planes of satellites in Λ CDM simulations are of a transient nature due to chance projections (see also Buck et al. 2016). They do not form co-rotating structures, otherwise we would expect to mock-observe a similar kinematic coherence from different directions. Therefore, the probability of having chance projections in the three nearest and best-studied satellite systems (Milky Way, Andromeda, and Cen A) appears arbitrarily small.

The central halos of the three simulated systems resembling the Cen A satellite population have varied merger histories. Two of them show quiescent growth over the last 10 Gyr, while one

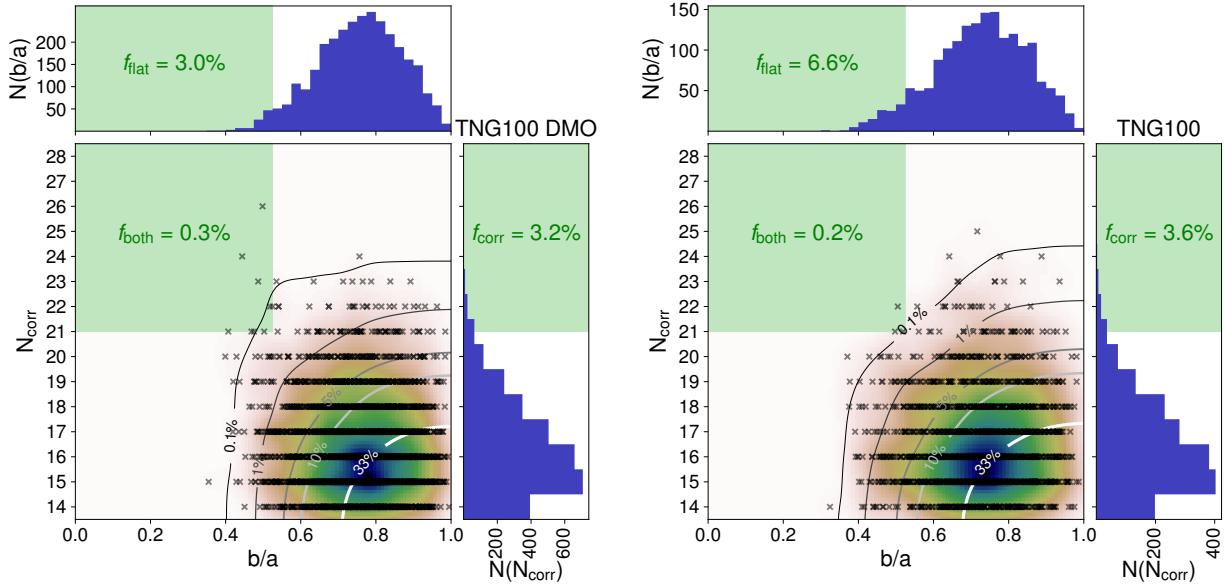


Fig. 3. Mock-observed satellite systems around Cen A analogs from the Illustris TNG-100 simulation, considering both its dark-matter-only run (*left*) and hydrodynamical run (*right*). The vertical axis plots the number of kinematically correlated satellites N_{corr} , with $N_{\text{corr}} = 21$ for the observed Cen A system. The horizontal axis plots the on-sky axis-ratio flattening b/a . The histograms show the number of realizations with a given axis ratio $N(b/a)$ and a given number of correlated velocities $N(N_{\text{corr}})$, respectively. The color maps indicate the density of simulated systems, while the contours indicate what fraction of simulated systems are more extreme than the parameter combination. The green shaded regions indicate parameter combinations that are as extreme or more as the observed Cen A system, while f_{flat} , f_{corr} , and f_{both} report the fraction of mock systems that are at least as flattened as the observed system, at least as kinematically correlated, or both simultaneously.

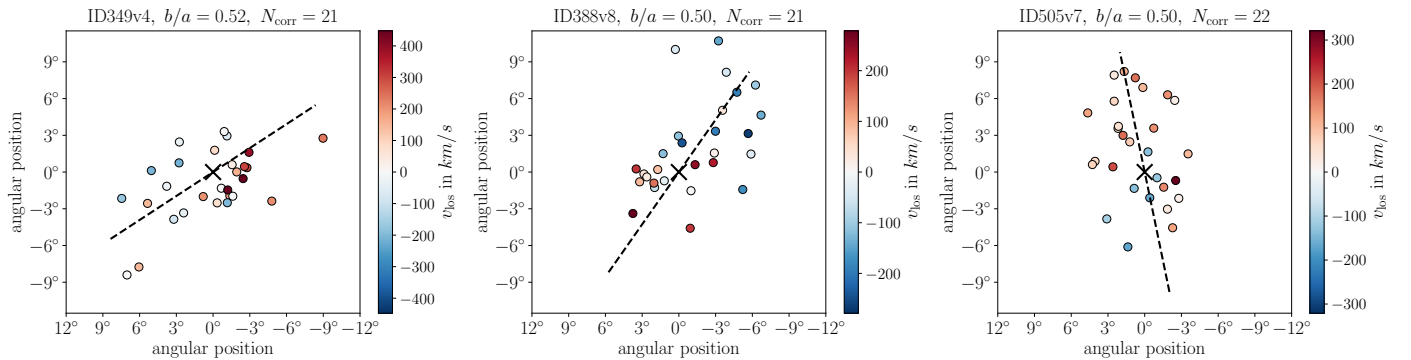


Fig. 4. Mock-observed on-sky satellite distributions of the three simulated systems that have satellite plane parameters as extreme as observed. The satellite galaxies (circles) are color coded by their line-of-sight velocity relative to the host (black cross). The dashed lines indicate the major axis of the projected distribution of satellites. The top labels give the minor-to-major axis flattening b/a of the on-sky distribution for the simulated systems, as well as the number of correlated velocities N_{corr} .

experienced a major merger 4 Gyr ago. The high coherence in the latter’s satellites is unlikely to result from the merger event, contrary to what is proposed by [Smith et al. \(2016\)](#). Most of a major merger influence would have been washed out by the subsequent stripping of participating satellites and the accretion of new satellites (Kanehisa et al., in prep.). None of these three analogs match Cen A’s reported major merger 2 Gyr ago ([Wang et al. 2020](#)).

4. Summary and conclusions

The phase-space distribution of dwarf satellite galaxies provides a key test bed for cosmological predictions on small scales. For the Cen A system, it has been suggested based on 16 line-of-sight velocities ([Müller et al. 2018b](#)) that most dwarf galaxies are aligned in a co-rotating structure similar to what has been found for the MW and the Andromeda galaxy. We revis-

ited this issue by adding 12 more satellites of Cen A, for which we acquired line-of-sight velocities using MUSE spectroscopic observations ([Müller et al. 2021](#)). This increases the sample size from 16 to 28 satellites and enhances the representation of gas-poor dwarf spheroidal galaxies.

We find that 21 out of 28 satellites show a coherent motion. This implies that the co-moving satellite system inferred around Cen A was not a chance occurrence due to the small number of tracers, but it is a real phenomenon.

In the Illustris-TNG simulation, satellite systems that are at least as flattened and kinematically correlated as Cen A occur with a frequency of only 0.2% in the hydrodynamical and 0.3% in the DMO run. This indicates that the plane-of-satellites problem is independent of baryon physics. The simulated satellite systems that are consistent with the observed Cen A properties are not stable, co-rotating structures: their kinematic coherence arises by chance projection.

In summary, we find that the additional kinematic data obtained for 12 more Cen A satellites (Müller et al. 2021) does not alleviate the tension with Λ CDM expectations. The new velocities further support the findings of Müller et al. (2018b). The satellite system of Cen A remains a challenge for Λ CDM.

Acknowledgements. We thank the referee for the constructive report, which helped to clarify and improve the manuscript. O.M. is grateful to the Swiss National Science Foundation for financial support. M.S.P. and O.M. thank the DAAD for PPP grant 57512596 funded by the BMBF, and the Partenariat Hubert Curien (PHC) for PROCOPE project 44677UE. M.S.P. thanks the Klaus Tschira Stiftung gGmbH and German Scholars Organization e.V. for support via a Klaus Tschira Boost Fund. H.J. acknowledges financial support from the Australian Research Council through the Discovery Project DP150100862. N.L. acknowledges financial support of the Project IDEXLYON at the University of Lyon under the Investments for the Future Program (ANR-16-IDEX-0005).

References

- Banks, G. D., Disney, M. J., Knezek, P. M., et al. 1999, *ApJ*, **524**, 612
- Bouchard, A., Jerjen, H., Da Costa, G. S., & Ott, J. 2007, *AJ*, **133**, 261
- Boylan-Kolchin, M., Springel, V., White, S. D. M., Jenkins, A., & Lemson, G. 2009, *MNRAS*, **398**, 1150
- Buck, T., Dutton, A. A., & Macciò, A. V. 2016, *MNRAS*, **460**, 4348
- Cautun, M., Wang, W., Frenk, C. S., & Sawala, T. 2015, *MNRAS*, **449**, 2576
- Crnojević, D., Sand, D. J., Spekkens, K., et al. 2016, *ApJ*, **823**, 19
- Crnojević, D., Sand, D. J., Bennet, P., et al. 2019, *ApJ*, **872**, 80
- Dinescu, D. I., Keeney, B. A., Majewski, S. R., & Girard, T. M. 2004, *AJ*, **128**, 687
- Doyle, M. T., Drinkwater, M. J., Rohde, D. J., et al. 2005, *MNRAS*, **361**, 34
- Ibata, R. A., Lewis, G. F., Conn, A. R., et al. 2013, *Nature*, **493**, 62
- Ibata, R. A., Ibata, N. G., Lewis, G. F., et al. 2014a, *ApJ*, **784**, L6
- Ibata, N. G., Ibata, R. A., Famaey, B., & Lewis, G. F. 2014b, *Nature*, **511**, 563
- Ibata, R. A., Famaey, B., Lewis, G. F., Ibata, N. G., & Martin, N. 2015, *ApJ*, **805**, 67
- Jerjen, H., Freeman, K. C., & Binggeli, B. 2000a, *AJ*, **119**, 166
- Jerjen, H., Binggeli, B., & Freeman, K. C. 2000b, *AJ*, **119**, 593
- Karachentsev, I. D., Karachentseva, V. E., Huchtmeier, W. K., & Makarov, D. I. 2004, *AJ*, **127**, 2031
- Karachentsev, I. D., Tully, R. B., Dolphin, A., et al. 2007, *AJ*, **133**, 504
- Karachentsev, I. D., Makarov, D. I., & Kaisina, E. I. 2013, *AJ*, **145**, 101
- Kirby, E. M., Koribalski, B., Jerjen, H., & López-Sánchez, Á. 2012, *MNRAS*, **420**, 2924
- Koch, A., & Grebel, E. K. 2006, *AJ*, **131**, 1405
- Koribalski, B. S., Staveley-Smith, L., Kilborn, V. A., et al. 2004, *AJ*, **128**, 16
- Kroupa, P., Theis, C., & Boily, C. M. 2005, *A&A*, **431**, 517
- Kunkel, W. E., & Demers, S. 1976, in *The Galaxy and the Local Group*, eds. R. J. Dickens, J. E. Perry, F. G. Smith, & I. R. King, *Royal Greenwich Observatory Bulletins*, **182**, 241
- Libeskind, N. I., Frenk, C. S., Cole, S., et al. 2005, *MNRAS*, **363**, 146
- Libeskind, N. I., Frenk, C. S., Cole, S., Jenkins, A., & Helly, J. C. 2009, *MNRAS*, **399**, 550
- Libeskind, N. I., Yepes, G., Knebe, A., et al. 2010, *MNRAS*, **401**, 1889
- Libeskind, N. I., Hoffman, Y., Tully, R. B., et al. 2015, *MNRAS*, **452**, 1052
- Libeskind, N. I., Guo, Q., Tempel, E., & Ibata, R. 2016, *ApJ*, **830**, 121
- Libeskind, N. I., Carlesi, E., Müller, O., et al. 2019, *MNRAS*, **490**, 3786
- Lipnicky, A., & Chakrabarti, S. 2017, *MNRAS*, **468**, 1671
- Lynden-Bell, D. 1976, *MNRAS*, **174**, 695
- Lynden-Bell, D. 1982, *The Observatory*, **102**, 202
- McConnachie, A. W., & Irwin, M. J. 2006, *MNRAS*, **365**, 902
- Metz, M., Kroupa, P., & Libeskind, N. I. 2008, *ApJ*, **680**, 287
- Müller, O., Jerjen, H., & Binggeli, B. 2015, *A&A*, **583**, A79
- Müller, O., Jerjen, H., Pawlowski, M. S., & Binggeli, B. 2016, *A&A*, **595**, A119
- Müller, O., Scalera, R., Binggeli, B., & Jerjen, H. 2017a, *A&A*, **602**, A119
- Müller, O., Jerjen, H., & Binggeli, B. 2017b, *A&A*, **597**, A7
- Müller, O., Rejkuba, M., & Jerjen, H. 2018a, *A&A*, **615**, A96
- Müller, O., Pawlowski, M. S., Jerjen, H., & Lelli, F. 2018b, *Science*, **359**, 534
- Müller, O., Rejkuba, M., Pawlowski, M. S., et al. 2019, *A&A*, **629**, A18
- Müller, O., Fahrion, K., Rejkuba, M., et al. 2021, *A&A*, in press, <https://doi.org/10.1051/0004-6361/202039359>
- Nelson, D., Springel, V., Pillepich, A., et al. 2019, *Comput. Astrophys. Cosmol.*, **6**, 2
- Pawlowski, M. S. 2018, *Mod. Phys. Lett. A*, **33**, 1830004
- Pawlowski, M. S., & Kroupa, P. 2020, *MNRAS*, **491**, 3042
- Pawlowski, M. S., Pflamm-Altenburg, J., & Kroupa, P. 2012, *MNRAS*, **423**, 1109
- Pawlowski, M. S., Famaey, B., Merritt, D., & Kroupa, P. 2015, *ApJ*, **815**, 19
- Pawlowski, M. S., Bullock, J. S., Kelley, T., & Famaey, B. 2019, *ApJ*, **875**, 105
- Peterson, R. C., & Caldwell, N. 1993, *AJ*, **105**, 1411
- Phillips, J. I., Cooper, M. C., Bullock, J. S., & Boylan-Kolchin, M. 2015, *MNRAS*, **453**, 3839
- Pillepich, A., Nelson, D., Hernquist, L., et al. 2018, *MNRAS*, **475**, 648
- Planck Collaboration XIII. 2016, *A&A*, **594**, A13
- Puzia, T. H., & Sharina, M. E. 2008, *ApJ*, **674**, 909
- Samuel, J., Wetzel, A., Chapman, S., et al. 2020, *MNRAS*, submitted [arXiv:2010.08571]
- Santos-Santos, I., Dominguez-Tenreiro, R., Artal, H., et al. 2020, *ApJ*, **897**, 71
- Saviane, I., & Jerjen, H. 2007, *AJ*, **133**, 1756
- Sawala, T., Frenk, C. S., Fattahi, A., et al. 2016, *MNRAS*, **457**, 1931
- Smith, R., Duc, P. A., Bournaud, F., & Yi, S. K. 2016, *ApJ*, **818**, 11
- Sohn, S. T., Patel, E., Besla, G., et al. 2017, *ApJ*, **849**, 93
- Sohn, S. T., Patel, E., Fardal, M. A., et al. 2020, *ApJ*, **901**, 43
- Springel, V., White, S. D. M., Jenkins, A., et al. 2005, *Nature*, **435**, 629
- Springel, V., Pakmor, R., Pillepich, A., et al. 2018, *MNRAS*, **475**, 676
- Taylor, M. A., Eigenthaler, P., Puzia, T. H., et al. 2018, *ApJ*, **867**, L15
- Tully, R. B., Shaya, E. J., Karachentsev, I. D., et al. 2008, *ApJ*, **676**, 184
- Tully, R. B., Libeskind, N. I., Karachentsev, I. D., et al. 2015, *ApJ*, **802**, L25
- Vogelsberger, M., Genel, S., Springel, V., et al. 2014, *MNRAS*, **444**, 1518
- Wang, J., Hammer, F., Rejkuba, M., Crnojević, D., & Yang, Y. 2020, *MNRAS*, **498**, 2766
- Zentner, A. R., Kravtsov, A. V., Gnedin, O. Y., & Klypin, A. A. 2005, *ApJ*, **629**, 219

Appendix A: Table

Table A.1. Members of Cen A used in this study.

Galaxy name	Alternative name	α_{2000} (°)	δ_{2000} (°)	D (Mpc)	v_h (km s ⁻¹)	Source	Type
(a)	(b)	(c)	(d)	(e)	(f)	(g)	(h)
ESO 269–037	PGC045916	195.8875	−46.5842	3.15 ± 0.09 (1)	744 ± 2 (2)	HI	dIrr
NGC 4945	PGC045279	196.3583	−49.4711	3.72 ± 0.03 (3)	563 ± 3 (4)	HI	Scd
ESO 269–058	PGC045717	197.6333	−46.9908	3.75 ± 0.02 (1)	400 ± 18 (5)	HI	dIrr
KK 189	PGC166158	198.1883	−41.8320	4.21 ± 0.17 (6)	753 ± 4 (7)	Stars	dSph
ESO 269–066	PGC045916	198.2875	−44.8900	3.75 ± 0.03 (1)	784 ± 31 (8)	Stars	dSph
NGC 5011C	PGC045917	198.2958	−43.2656	3.73 ± 0.03 (1)	647 ± 96 (9)	Stars	Tr
KKs 54	PGC2815821	200.3829	−31.8864	3.75 ± 0.10 (10)	621 ± 11 (7)	Stars	Tr
KK 196	PGC046663	200.4458	−45.0633	3.96 ± 0.11 (1)	741 ± 15 (11)	Stars	dIrr
NGC 5102	PGC046674	200.4875	−36.6297	3.74 ± 0.39 (3)	464 ± 18 (12)	HI	Sa
KK 197	PGC046680	200.5086	−42.5359	3.84 ± 0.04 (1)	643 ± 3 (7)	Stars	dSph
KKs 55	PGC2815822	200.5500	−42.7311	3.85 ± 0.07 (1)	530 ± 14 (7)	Stars	Sph
dw1322–39		200.6336	−39.9060	2.95 ± 0.05 (10)	656 ± 10 (7)	Stars	dIrr
dw1323–40b		200.9809	−40.8361	3.91 ± 0.61 (10)	497 ± 12 (7)	Stars	dSph
dw1323–40a		201.2233	−40.7612	3.73 ± 0.15 (10)	450 ± 14 (7)	Stars	dSph
Cen A	PGC046957	201.3667	−43.0167	3.68 ± 0.05 (1)	556 ± 10 (4)	HI	S0 ⁰
KK 203	PGC166167	201.8681	−45.3524	3.78 ± 0.25 (3)	306 ± 10 (7)	Stars	Tr
ESO 324–024	PGC047171	201.9042	−41.4806	3.78 ± 0.09 (1)	514 ± 18 (12)	HI	Sdm
NGC 5206	PGC047762	203.4292	−48.1511	3.21 ± 0.01 (1)	583 ± 6 (13)	stars	S0 [−]
NGC 5237	PGC048139	204.4083	−42.8475	3.33 ± 0.02 (1)	361 ± 4 (4)	HI	BCD
NGC 5253	PGC048334	204.9792	−31.6400	3.55 ± 0.03 (3)	407 ± 3 (4)	HI	Sdm
dw1341–43		205.4032	−43.8553	3.53 ± 0.04 (10)	636 ± 14 (7)	Stars	dSph
KKs 57	PGC2815823	205.4079	−42.5797	3.84 ± 0.47 (1)	511 ± 17 (7)	Stars	Sph
KK 211	PGC048515	205.5208	−45.2050	3.68 ± 0.14 (1)	600 ± 31 (14)	Stars	Sph
dw1342–43		205.6837	−43.2548	2.90 ± 0.14 (10)	510 ± 8 (7)	Stars	Tr
ESO 325–011	PGC048738	206.2500	−41.8589	3.40 ± 0.05 (1)	544 ± 1 (15)	HI	dIrr
KKs 58	PGC2815824	206.5031	−36.3289	3.36 ± 0.10 (10)	477 ± 5 (7)	Stars	dSph
KK 221	PGC166179	207.1917	−46.9974	3.82 ± 0.07 (1)	507 ± 13 (14)	Stars	dIrr
ESO 383–087	PGC049050	207.3250	−36.0614	3.19 ± 0.03 (1)	326 ± 2 (4)	HI	Sdm
ESO174–001/KKs 57	PGC048937	206.9920	−53.3476	$3.68^{(*)}$	686 ± 1 (15)	HI	dIrr

Notes. (a) Galaxy name, (b) Alternative PGC name, (c) Right ascension in epoch J2000, (d) Declination in epoch J2000, (e) Galaxy distance, and reference for the distance measurement, (f) Galaxy heliocentric velocity and reference for the velocity measurement, (g) The technique of the velocity measurement, and (h) de Vaucouleurs morphological type according to the Local Volume catalog (Karachentsev et al. 2004, 2013). ^(*)For ESO174–001/KKs 57, no accurate TRGB distance is available, therefore we assigned the measured distance of Cen A to this dwarf galaxy.

References. (1) Karachentsev et al. (2013), (2) Bouchard et al. (2007), (3) Tully et al. (2015), (4) Koribalski et al. (2004), (5) Banks et al. (1999), (6) Tully et al. (2008), (7) Müller et al. (2021), (8) Jerjen et al. (2000a), (9) Saviane & Jerjen (2007), (10) Müller et al. (2019), (11) Jerjen et al. (2000b), (12) Doyle et al. (2005), (13) Peterson & Caldwell (1993), (14) Puzia & Sharina (2008), and (15) Kirby et al. (2012).